Pergamon

Acta mater. Vol. 46, No. 2, pp. 639–649, 1998

Printed in Great Britain
PII: S1359-6454(97)00241-3
1359-6454/98 $19.00 + 0.00

MORPHOLOGICAL EVOLUTION OF COHERENT MULTI-VARIANT $Ti_{11}Ni_{14}$ PRECIPITATES IN Ti-Ni ALLOYS UNDER AN APPLIED STRESS—A COMPUTER SIMULATION STUDY

D. Y. LI and L. Q. CHEN

Department of Materials Science & Engineering, The Pennsylvania State University, University Park, PA 16802, USA

(Received 28 January 1997; accepted 25 June 1997)

Abstract—Coherent precipitation of multi-variant $Ti_{11}Ni_{14}$ precipitates in TiNi alloys was investigated by employing a continuum field kinetic model. The structural difference between the precipitate phase and the matrix as well as the orientational differences between precipitate variants are distinguished by nonconserved structural field variables, whereas the compositional difference between the precipitate and matrix is described by a conserved field variable. The temporal evolution of the spatially dependent field variables is determined by numerically solving the time-dependent Ginzburg–Landau (TDGL) equations for the structural variables and the Cahn–Hilliard diffusion equation for the composition. In particular, the interaction between precipitates, and the growth morphology of $Ti_{11}Ni_{14}$ precipitates *under strain-constraints* were studied, without *a priori* assumptions on the precipitate shape and distribution. The predicted morphology and distribution of $Ti_{11}Ni_{14}$ variants were compared with experimental observations. Excellent agreement between the simulation and experimental observations was found. © *1998 Acta Metallurgica Inc.*

1. INTRODUCTION

A coherent phase transformation with a point symmetry reduction usually produces a number of variants which are oriented in different, but equivalent crystallographic directions. For example, $Ti_{11}Ni_{14}$ precipitate in a Ni-rich TiNi alloy has a rhombohedral structure, and it has eight variants whose $(111)_{Ti_{11}Ni_{14}}$ planes are, respectively parallel to $\{111\}_{B2}$ of the ordered BCC TiNi matrix (B2 structure) [1, 2]. The eight variants fall into four groups and each group includes a pair of conjugate variants which can be obtained from each other by a 180° rotation operation (e.g. $(111)_{Ti_{11}Ni_{14}} \| (111)_{B2}$ variant and $(111)_{Ti_{11}Ni_{14}} \| (\bar{1}\bar{1}\bar{1})_{B2}$ variant). If an initial homogeneous TiNi alloy is aged within the two-phase region of $Ti_{11}Ni_{14}$ and TiNi without any external constraint, all the differently oriented variants will grow with the same probability.

Coherent variants usually exhibit non-spherical shapes due to the anisotropically elastic interactions arising from the lattice mismatch between the precipitate phase and the matrix [3, 4]. For instance, the coherent $Ti_{11}Ni_{14}$ precipitates have a near lens-like shape. Furthermore, during precipitation, different variants arrange in such a way that the overall strain energy caused by the variants is minimized, leading to a so-called self-accommodative arrangement of precipitate variants. However, if an external strain or stress is applied during ageing, only some of the variants are favored to grow. As a result, an anistropic distribution of precipitate variants can be attained and this may result in unique properties of the material. In Ti–Ni binary alloy with 57.0 wt%–57.5 wt% Ni, it was found that, under a constant stress or strain constraint, only one type variant grows selectively, producing a two-phase microstructure with the coherent $Ti_{11}Ni_{14}$ precipitates aligned in parallel. These lenticular precipitates aligned in parallel result in an excellent two-way shape memory effect, called all-round shape memory effect (ARSME) [1, 5, 6].

The main objective of this simulation study is to investigate coherent $Ti_{11}Ni_{14}$ precipitation in a supersaturated TiNi matrix and effects of applied strain-constraints on the growth and distribution of differently oriented $Ti_{11}Ni_{14}$ variants. A continuum diffuse-interface field model based on the time-dependent Ginzburg–Landau and Cahn–Hilliard diffusion equations was employed. The morphology and growth behavior of a single $Ti_{11}Ni_{14}$ variant has been studied previously [7]. The main focus of this paper is on the interactions between precipitate variants and the temporal evolution of *multi-variant* microstructure under applied strain-constraints. The simulation of a multi-variant system under strain-constraint may help us to further understand the constraint effect on precipitation behavior, which is helpful for designing adequate thermomechanical treatments to obtain optimal microstructure.

2. DESCRIPTION OF A MULTI-VARIANT TWO-PHASE MICROSTRUCTURE

In the diffuse-interface field model, a microstructure is described by a set of spatially dependent field variables. Since the precipitates ($Ti_{11}Ni_{14}$) and matrix (NiTi) differ not only in composition but also in structure, description of a two-phase mixture requires fields of both concentration $C(\mathbf{r}, t)$ and long-range structural order parameters $\eta_i(\mathbf{r}, t)$ where subscript, i, corresponds to differently oriented variant of the precipitate phase. The concentration field describes the compositional difference between the precipitate phase and the matrix, while the structural order parameter fields distinguish the structural difference between the precipitate and the matrix and also distinguish differently oriented variants of the precipitate. These field variables are continuous across the interphase boundaries.

3. THE DRIVING FORCE FOR MICROSTRUCTURAL EVOLUTION

The driving force for the temporal evolution of a coherent microstructure consists of the following: (i) reduction in the bulk chemical free energy, (ii) decrease of the total interfacial energy of the boundaries between different phases or between differently oriented variants, (iii) relaxation of the elastic strain energy caused by the lattice mismatch between the matrix and the precipitate phase and (iv) external loads, i.e. a constant applied strain or stress. We need to express all the contributions to the driving force in terms of the field variables.

3.1. The bulk chemical free energy

The growth of $Ti_{11}Ni_{14}$ precipitates is driven by the difference in chemical free energy between the supersaturated TiNi matrix and the equilibrium TiNi matrix containing the $Ti_{11}Ni_{14}$ precipitates. In the field model, the local "chemical" free energy density is approximated using a Landau-type of free energy polynomial

$$f(C,\eta_p)=\frac{A_1}{2}(C-C_1)^2+\frac{A_2}{2}(C-C_2)\sum_p^v\eta_p^2-\frac{A_3}{4}\sum_p^v\eta_p^4+\frac{A_4}{6}\sum_p^v\eta_p^6+A_5\sum_{q\neq p}^v\eta_p^2\eta_q^2+A_6\sum_{p\neq q,p\neq r}^v\eta_p^4(\eta_q^2+\eta_r^2)+A_7\sum_{p\neq q\neq r}^v\eta_p^2\eta_q^2\eta_r^2 \quad (1)$$

where, v is the number of orientation variants. If values of all the structural order parameter field variables are zero, it describes the dependence of the free energy of the matrix phase on composition. At a given composition, the local free energy function has v number of degenerate minima corresponding to the free energy of each orientation variant. Therefore, the free energy density as a function of composition for the precipitate phase can be obtained by minimizing f with respect to the order field variables at different compositions, i.e. $f(C, \eta_{io}(C))$. For the particular case of $Ti_{11}Ni_{14}$ precipitation from a TiNi matrix, the coefficients in Equation (1) were chosen as follows: $A_1 = 65.00$, $A_2 = 7.54$, $A_3 = 1.50$, $A_4 = 1.45$, and $A_5 = A_6 = A_7 = 0.2$. (The free energy was measured in a unit, $mk_BT \approx 10^8$ ergs/cm^3, where $T = 773$°C, m is a normalization coefficient.) $C_1 = 0.44$ and $C_2 = 0.38$ are constants which are close to equilibrium concentrations of the matrix and the precipitate phase, respectively. Figure 1 illustrates the chemical free energy as a function of C: one curve corresponds to the TiNi matrix (B2 phase) and the other corresponds to the $Ti_{11}Ni_{14}$ precipitate phase. It should be noted that the energy curves used here is only an approximation to actual chemical free energy of the system. For the present simulation, the accuracy of the chemical free energy is not critical as long as it provides correct equilibrium compositions and the driving force for precipitation.

3.2. The interfacial energy

In addition to the chemical free energy, the interphase boundary energy also contributes to the system's total free energy. In this work, isotropic interfacial energy is assumed and introduced through the gradient terms in C and η_p. The total chemical free energy of an inhomogeneous system may be expressed as [8, 9]

$$F_c=\int_V\left[f(C,\eta_p(\mathbf{r}))+\sum_{p=1}^v\frac{\alpha_p}{2}(\nabla\eta_p(\mathbf{r}))^2+\frac{\beta}{2}(\nabla C)^2\right]d^3\mathbf{r} \quad (2)$$

where α_p and β are gradient energy coefficients. The integration is performed over the entire system. The total interfacial energy of the system is then defined as the excess free energy associated with the interfaces, i.e.

$$\sigma_{tot}=\int\left[f(C,\eta_i)-f_o(C)+\sum_{i=1}^v\frac{\alpha_i}{2}(\nabla\eta_i)^2+\frac{\beta}{2}(\nabla C)^2\right]d^3\mathbf{r} \quad (3)$$

where

$$f_o(C)=f_{Ti_{11}Ni_{14}}(C_p,\eta_{io}(C_p))+\frac{f_{Ti_{11}Ni_{14}}(C_p,\eta_{io}(C_p))-f_{TiNi}(C_m,\eta_i=0)}{C_p-C_m}(C_o-C_p) \quad (4)$$

where C_p and C_m are compositions of the precipi-

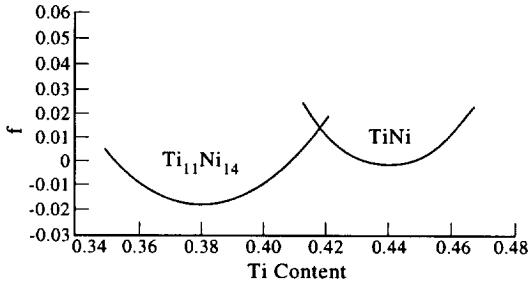

Fig. 1. Specific free energy vs concentration for TiNi (B2) phase and $Ti_{11}Ni_{14}$ phase, calculated using Equation (1) with $A_1 = 65.00$, $A_2 = 7.54$, $A_3 = 1.50$, $A_4 = 1.45$, and $A_5 = A_6 = A_7 = 0.2$.

tate and the matrix, respectively. C_o is the average composition of the system.

3.3. *Elastic strain energy*

For coherent precipitates, an important contribution to the total free energy comes from the strain energy caused by the lattice mismatch between the $Ti_{11}Ni_{14}$ precipitate and the TiNi matrix. Equilibrium TiNi alloy has a B2 structure (i.e. ordered BCC structure, $a_0 = 3.01$ Å) [10], while $Ti_{11}Ni_{14}$ precipitate phase has a rhombohedral structure ($a_0 = 6.72$ Å, $\gamma = 113.9°$) [11, 12]. The morphology (shape and orientation) of a coherent precipitate variant is determined by the balance between the strain energy and the interphase boundary energy.

Calculation of the strain energy of a coherent precipitate was pioneered by Eshelby [13, 14], who derived equations of the elastic strain of an ellipsoidal inclusion in an isotropic matrix based on the assumption that both phases have the same elastic moduli. A general theory of elastic strain energy of a coherent two-phase system with arbitrary morphology in the homogeneous modulus approximation was proposed later by Khachaturyan [15]. In Khachaturyan's theory, the exact equation for strain energy and the Fourier transform of elastic displacement in an arbitrary two-phase coherent mixture were derived. This theory was then extended to arbitrary coherent mixtures comprising inclusions formed by crystal lattice rearrangements of different types [16], using which, one may obtain all the results of Eshelby theory for ellipsoidal inclusions in isotropic matrices. In the meantime, Eshelby theory was also modified, extended, and developed by many researchers [17–22]. Walpole [17], Kinoshita and Mura [18], and Asaro and Barnett [19] subsequently proved or extended Eshebly theory to the anisotropic elastic cases. Lee *et al.* [21] obtained the solution of the anisotropic elastic strain energy of coherent ellipsoidal precipitates. Since the assumption of elastic homogeneity is not suitable for describing some coherent microstructures, e.g. ($\gamma' + \gamma$) two-phase microstructure of a Ni-based superalloy with a pure dilatational lattice mismatch, efforts are therefore made to extend the elastic theories for analyzing microstructural evolution in elastically inhomogeneous solids. A recent paper [23] reports on the extension of Khachaturyan theory to elastically inhomogeneous cases.

In general, the degree of lattice mismatch between precipitates and the matrix is characterized by the stress-free transformation strain which is nonzero only within the precipitates and may be represented as

$$\varepsilon_{ij}^{\circ} = \frac{a_p - a_m}{a_m}$$

where a_p and a_m are the lattice parameters of a precipitate variant p and the matrix phase, respectively. In the sharp-interface description of a two-phase microstructure, the spatial dependence of the stress-free strain can be characterized by a so-called shape-function which is 1 within a precipitate and 0 in the matrix.

In the diffuse-interface description, however, we have to express the stress-free strain in terms of field variables. Let's assume that the local stress-free transformation strain, $\varepsilon_{ij}^{\circ}(\mathbf{r})$, is primarily dependent on the structural order parameter through

$$\varepsilon_{ij}^{\circ}(\mathbf{r}) = \sum_p \varepsilon_{ij}^{\circ}(p)\eta_p^2(\mathbf{r}) \tag{5}$$

where $\eta_p(\mathbf{r})$ is the normalized structural order parameter describing the pth variant, and $\varepsilon_{ij}^{\circ}(p)$ is the corresponding stress-free strain for the pth variant when $\eta_p(\mathbf{r}) = 1$. The elastic energy in absence of applied stress or strain was previously obtained [9, 24, 25]. The Appendix presents a derivation of the elastic energy equation to make the paper self-contained.

When a precipitation process (i.e. ageing) is constrained by applying constant strain or stress, the coherent strain field caused by a precipitate is changed by the constraint strain or stress, and this results in a variation of the strain energy barrier to the growth of the precipitate. There are two types of constraints [7]. One is the *strain-constraint*, in which the system's boundary is fixed after applying an external force to the system, followed by the precipitation process. Under such a condition, the system is subjected to a constant external strain. The governing potential of the system is the Helmholtz free energy. The second type of constraint, called *stress-constraint*, is to apply a constant stress on the system without fixing the system's boundary. Under this condition, the system is subjected to a constant external force. In this case, the governing potential is the Gibbs free energy.

In the first case, since the boundary of the system is fixed, the total elastic energy is obtained by replacing the homogeneous strain in the elastic energy equation (Appendix (A13)) by the applied homo-

geneous strain, i.e. $\bar{\varepsilon}_{ij} = \varepsilon^{a}_{ij}$,

$$E^{\varepsilon}_{el} = \frac{V}{2} C_{ijkl}\varepsilon^{a}_{ij}\varepsilon^{a}_{kl} - VC_{ijkl}\varepsilon^{a}_{ij}\sum_{p}\varepsilon^{o}_{kl}(p)\overline{\eta^{2}_{p}(\mathbf{r})} + \frac{V}{2} C_{ijkl}\sum_{p}\sum_{q}\varepsilon^{o}_{ij}(p)\varepsilon^{o}_{kl}(q)\overline{\eta^{2}_{p}(\mathbf{r})\eta^{2}_{q}(\mathbf{r})} - \frac{1}{2}\sum_{p}\sum_{q}\int\frac{d^{3}\mathbf{g}}{(2\pi)^{3}} B_{pq}(\mathbf{n})\{\eta^{2}_{p}(\mathbf{r})\}^{*}_{\mathbf{g}}\{\eta^{2}_{q}(\mathbf{r})\}_{\mathbf{g}}$$

where the second term represents the coupling between the transformation strain, $\varepsilon^{o}_{ij}(p)$, and the constant applied strain, ε^{a}_{ij}.

For the second type of constraint, a constant homogeneous stress, σ^{a}_{ij}, or surface force, is applied to the system during precipitation process. The total energy (elastic energy + potential of the loading device) due to the transformation strain and the applied stress is given by

$$E = E_{el} - V\sigma^{a}_{ij}\bar{\varepsilon}_{ij} \tag{7}$$

where E_{el} is given by equation (A13) in the Appendix. By mimizing E with respect to $\bar{\varepsilon}_{ij}$

$$\frac{\partial E}{\partial\bar{\varepsilon}_{ij}} = VC_{ijkl}\bar{\varepsilon}_{kl} - VC_{ijkl}\sum_{p}\varepsilon^{o}_{kl}(p)\overline{\eta^{2}_{p}(\mathbf{r})} - V\sigma^{a}_{ij} = 0. \tag{8}$$

We obtain the homogeneous strain under the influence of an applied stress,

$$\bar{\varepsilon}_{ij} = S_{ijkl}\sigma^{a}_{kl} + \sum_{p}\varepsilon^{o}_{ij}(p)\overline{\eta^{2}_{p}(\mathbf{r})} \tag{9}$$

where S_{ijkl} is the compliance tensor. Substituting equation (9) back into the expression of E, we get the total elastic energy contribution (including the potential of external loading device) under the constant stress condition,

$$E^{\sigma}_{el} = \frac{V}{2} C_{ijkl}\sum_{p}\sum_{q}\varepsilon^{o}_{ij}(p)\varepsilon^{o}_{kl}(q)\left[\overline{\eta^{2}_{p}(\mathbf{r})\eta^{2}_{q}(\mathbf{r})} - \overline{\eta^{2}_{p}(\mathbf{r})}\;\overline{\eta^{2}_{q}(\mathbf{r})}\right] - \frac{1}{2}\sum_{p}\sum_{q}\int\frac{d^{3}\mathbf{g}}{(2\pi)^{3}} B_{pq}(\mathbf{n})\{\eta^{2}_{p}(\mathbf{r})\}^{*}_{\mathbf{g}}\{\eta^{2}_{p}(\mathbf{r})\}_{\mathbf{g}} - \frac{V}{2} S_{ijkl}\sigma^{a}_{ij}\sigma^{a}_{kl} - V\sigma^{a}_{ij}\sum_{p}\varepsilon^{o}_{ij}(p)\overline{\eta^{2}_{p}(\mathbf{r})}. \tag{10}$$

The last term in equation (10) is the coupling between the applied stress and the coherent strain of the system. Comparing with the strain constraint, one may notice that the coupling terms in both cases have similar expressions because $C_{ijkl}\varepsilon^{a}_{kl} = \sigma^{a}_{ij}$. However, in the strain-constraint case, the system is subjected to a constant applied strain and $\sigma^{a}_{ij} = C_{ijkl}\varepsilon^{a}_{kl}$ is only the initially applied stress which causes the strain, ε^{a}_{kl}. While in the stress-constraint case, the system is subjected to a constant stress, σ^{a}_{ij}.

4. THE KINETIC EQUATIONS FOR MICROSTRUCTURAL EVOLUTION

In the field model, the temporal evolution of a microstructure is determined by solving the time-dependent partial differential kinetic equations for the field variables. For the nonconserved structural parameters, they are described by the time-dependent Ginzburg–Landau equations [25, 26], whereas for the conserved composition field, it is governed by the Cahn–Hilliard nonlinear diffusion equation [27]:

$$\frac{\partial\eta_{p}(\mathbf{r}, t)}{\partial t} = -L\frac{\delta F}{\delta\eta_{p}(\mathbf{r}, t)}$$

$$\frac{\partial C(\mathbf{r}, t)}{\partial t} = M\nabla^{2}\frac{\delta F}{\delta C(\mathbf{r}, t)} \tag{11}$$

where the subscript p represents different type of variants, M and L are kinetic coefficients which characterize the atomic diffusivity and interface boundary mobility, F is the total free energy of the system which includes the bulk chemical free energy, the interfacial energy, and the elastic strain energy. The expression of F is dependent on the constraint condition. In the strain-constraint condition, F is the Helmholtz free energy whereas in the stress-constraint condition, F is the Gibbs free energy. Since the TiNi shape memory alloys are often aged under strain constraints for the two-way shape memory effect, the strain-constraint condition was considered in the present simulation study, i.e.

$$F = F_{c} + E_{el} \tag{12}$$

where F_{c} and E_{el} are calculated using equations (2) and (6), respectively.

The variational derivatives of the total free energy with respect to the compositional and structural field variables are

$$\frac{\delta F}{\delta C(\mathbf{r})} = \frac{\delta F_{C}}{\delta C(\mathbf{r})} + \frac{\delta E_{el}}{\delta C(\mathbf{r})} = A_{1}[C(\mathbf{r}) - C_{1}] + \frac{A_{2}}{2}\sum_{p}\eta^{2}_{p}(\mathbf{r}) - \beta\nabla^{2}C(\mathbf{r}) \tag{13}$$

$$\frac{\delta F}{\delta\eta_{p}(\mathbf{r})} = \frac{\delta F_{C}}{\delta\eta_{p}(\mathbf{r})} + \frac{\delta E_{el}}{\delta\eta_{p}(\mathbf{r})} \tag{14}$$

where

$$\frac{\delta F_{c}}{\delta\eta_{p}(\mathbf{r})} = \eta_{p}(\mathbf{r})\Big\{A_{2}(C - C_{2}) - A_{3}\eta^{2}_{p}(\mathbf{r}) + A_{4}\eta^{4}_{p}(\mathbf{r}) + 2A_{5}\sum_{q\neq p}\eta^{2}_{q}(\mathbf{r}) + 2A_{6}\Big[2\eta^{2}_{p}(\mathbf{r})\Big(\sum_{q\neq p}\eta^{2}_{q}(\mathbf{r})\Big) + \Big(\sum_{q\neq p}\eta^{4}_{q}(\mathbf{r})\Big)\Big] + 2A_{7}\sum_{q\neq r\neq p}\eta^{2}_{q}(\mathbf{r})\eta^{2}_{r}(\mathbf{r})\Big\} - \alpha_{p}\nabla^{2}\eta_{p}(\mathbf{r}) \tag{15}$$

$$\frac{\delta E_{el}}{\delta \eta_p} = 2\eta_p(\mathbf{r})\Bigg[- C_{ijkl}\varepsilon^{a}_{ij}\varepsilon^{o}_{kl}(p) + \sum_q \Bigg[C_{ijkl}\varepsilon^{o}_{ij}(p)\varepsilon^{o}_{kl}(q)\eta^2_q(\mathbf{r}) - \{B_{pq}(\mathbf{n})\{\eta^2_q(\mathbf{r})\}_{\mathbf{g}}\}_{\mathbf{r}}\Bigg]\Bigg] \tag{16}$$

where $\{B_{pq}(\mathbf{n})\{\eta^2_q(\mathbf{r})\}_{\mathbf{g}}\}_{\mathbf{r}}$ represents the inverse Fourier transform of $B_{pq}(\mathbf{n})\{\eta^2_q(\mathbf{r})\}_{\mathbf{g}}$.

5. RESULTS AND DISCUSSION

A global coordinate frame was chosen whose x, y, z axes are, respectively parallel to $[1\bar{1}0]_{B2}$, $[112]_{B2}$, and $[111]_{B2}$ of the TiNi (B2) matrix. It is also the variant coordinate for the $Ti_{11}Ni_{14}$ variant with its $(111)_{Ti_{11}Ni_{14}} \| (111)_{B2}$, in which the eigen-strain matrix of the variant is given by

$$\begin{pmatrix} 0.014 & 0 & 0 \\ 0 & 0.014 & 0 \\ 0 & 0 & -0.029 \end{pmatrix}. \tag{17}$$

The elastic constants of TiNi matrix and the $Ti_{11}Ni_{14}$ precipitate phase were assumed to be the same, and have the following values: $C_{11} = 1.62 \times 10^{12}$ ergs/cm^3, $C_{12} = 1.29 \times 10^{12}$ ergs/cm^3, and $C_{44} = 0.34 \times 10^{12}$ ergs/cm^3 [28]. Since the given elastic constants are valid only in the coordinate frame $(x'y'z')$ whose three axes are parallel to $[100]_{B2}$, $[010]_{B2}$, and $[001]_{B2}$, the elastic constants were converted to the coordinate frame (xyz) through the tensor transformation law [29]:

$$C_{ijkl} = S_{ii'}S_{jj'}S_{kk'}S_{ll'}C_{i'j'k'l'} \tag{18}$$

where, $S_{ii'}$ is the coordinate transformation matrix which relates the $x'y'z'$ cooridinate to the xyz coordinate frame.

The eigen-strain matrix of a variant oriented in another $<111>_{B2}$ direction has the same expression in its own coordinate frame (say, frame s), and its form in the coordinate frame of a different variant (e.g. frame q) can be obtained through the tensor transformation law [29]

$$(\varepsilon^{o}_{ij})_q = S_{i_q i_s}S_{j_q j_s}(\varepsilon^{o}_{ij})_s \tag{19}$$

where, $S_{i_q i_s}$ is the transformation matrix which relates the $(xyz)_s$ frame to the $(xyz)_q$ frame.

The simulation was conducted in a two-dimensional space and four $Ti_{11}Ni_{14}$ variants were considered, which were distinguished by using two structural field variables ($\eta_1 = \pm\eta_o$ and $\eta_2 = \pm\eta_o$, respectively). A 200×200 uniform square grid was used to spatially discretize the field equations. The gradient coefficients α_p and β were assumed to be 2.0. L and M were chosen to be 0.2. In order to investigate the strain effect on the growth of $Ti_{11}Ni_{14}$ particles, compressive and tensile stresses, $\sigma = \mp 8(\times 10^8$ ergs/cm$^3) = \mp 80$ MPa, were initially applied to the system to introduce compressive and tensile strain constraints (i.e. resulted in constraint strain ε^a), respectively. Since both types of the evolution equations (see equation (11)) are nonlinear with respect to the field variables, they can only be solved numerically. A recently developed semi-implicit Fourier Spectral method [30] was used in the present simulation to solve these equations. Reduced time $t^* = t/t_o$ was used to represent the "ageing time", where $t_o = (Lmk_BT)^{-1}$. For each iteration, the time step is $\Delta t^* = 0.02$.

5.1. Two-particle interactions

It has been demonstrated in a previous paper [7] that a $Ti_{11}Ni_{14}$ precipitate has a lens-like shape with its normal parallel to $<111>_{B2}$ directions of the matrix. The morphology of a coherent precipitate is determined by the balance between the strain energy and the interphase boundary energy. When an external strain is applied, the coupling between the applied strain and the local strain may favor or unfavor the growth of the precipitate, depending on both the strain type (i.e. tension or compression) and its applying direction. When there is more than one particle present in a system, they will interact on each other through their long-range elastic fields. To study the inter-particle interactions, we first examine the interaction between two particles which belong to the same orientation variant described by the same structural order parameter $\eta_1 = \eta_o$. Figure 2 illustrates the growth of a pair of $Ti_{11}Ni_{14}$ variants whose $[111]_{Ti_{11}Ni_{14}}$ parallel to $[111]_{B2}$ direction. During growth, both of them changed their initially circular shape to a lens-like shape with bamboo leaf-like cross-section. This shape change is apparently induced by the coherent elastic strain since the interfacial energy is assumed to be isotropic. As the two particles impinged each other, they coalesced and formed a single domain.

The situation changes when the two particles belong to different orientation variant groups. Figure 3 illustrates the growth of a pair of conjugate particles whose $[111]_{Ti_{11}Ni_{14}}$ axes are respectively parallel to $[111]_{B2}$ and $[\bar{1}\bar{1}\bar{1}]_{B2}$ (distinguished by using $\eta_1 = \eta_o$ and $\eta_1 = -\eta_o$). During growth and impingement, the two particles did not coalesce, but formed a precipitate consisting of two antiphase domains separated by an antiphase boundary. The simulated coalescence and the formation of antiphase domains are consistent with TEM observation [2] which demonstrates that a $Ti_{11}Ni_{14}$ precipitate may consists of antiphase domains whose $[111]_{Ti_{11}Ni_{14}}$ are oriented in opposite $<111>_{B2}$ directions. Although morphologies of conjugate $Ti_{11}Ni_{14}$ variants are the same (both of them have the same eigen-strain matrix), their arrangement of atoms in a unit cell may be different in the global frame coordinate (needs a 180° rotation operation to change from one to the other [2]).

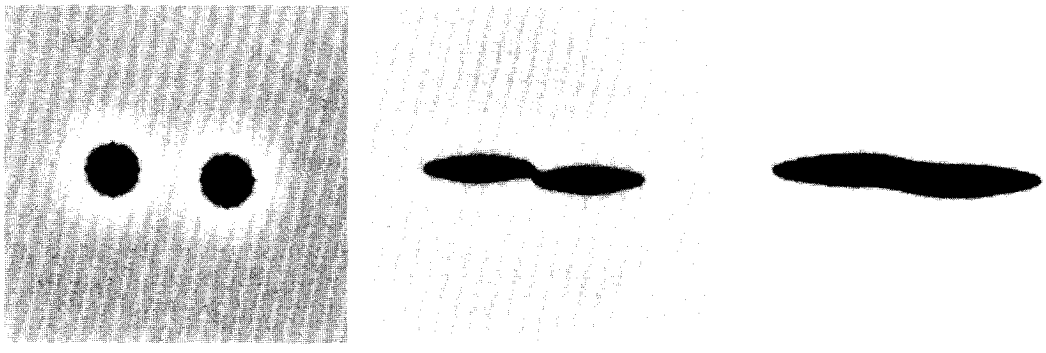

Fig. 2. The growth of a pair of $[111]_{Ti_{11}Ni_{14}} \| [111]_{B2}$ oriented $Ti_{11}Ni_{14}$ variant particles. The particles changed their shapes from spheres (circles in 2D) to lens-like plates with a bamboo leaf-like cross-section during growth, and they coalesced when contacting each other. (a) $t^* = 0$, (b) $t^* = 1.9 \times 10^3$, (c) $t^* = 4.7 \times 10^3$.

Figure 4 (a)–(c) illustrates the case of two variants whose $[111]_{Ti_{11}Ni_{14}}$ respectively parallel to $[111]_{B2}$ and $[11\bar{1}]_{B2}$ (distinguished by using $\eta_1 = \eta_0$ and $\eta_2 = \eta_0$). In this case, their eigen-strain matrices are different in the frame coordinate. As a result, they grew preferentially in different directions. They did not coalesce either because they belong to different orientation variant groups.

The main concern of this work is to examine the effect of strain-constraint on $Ti_{11}Ni_{14}$ precipitation. Simulation was conducted on the growth behavior of the two particles shown in Fig. 4(a) under applied tensile and compressive strains, respectively. The strains were applied along the x-axis (horizontally). Figure 4(e) demonstrates that under a compressive strain-constraint, the variant which is nearly perpendicular to the x-axis grew preferentially, while the other variant was retarded. The effect of the tensile strain-constraint is opposite to that of the compressive constraint. Under the tensile constraint, the variant which grew horizontally was favored, while the other was retarded (see Fig. 4(d)). This effect of strain-constraint comes from the coupling term, $-VC_{ijkl}e^a_{ij}\sum_p e^o_{kl}(p)\overline{\eta_p^2(\mathbf{r})}$, in the equation (6). Since differently oriented variants have different eigen-strain (in the global frame coordinate), this coupling term has different values for different variants and thus modifies the energy-barrier, caused by the coherent strain, to the growth of differently oriented variants. As a result, the growth of the precipitate variants becomes selective.

5.2. Microstructural evolution in multi-variant systems and the selective variant growth

Microstructural evolution in multi-variant systems was investigated. To begin with, the multi-variant $Ti_{11}Ni_{14}$ precipitation without applying strain constraints was simulated. Figure 5 illustrates the microstructural development of a multi-variant $Ti_{11}Ni_{14}$–TiNi system with an increase in the "ageing" time. The initial microstructure of the system was formed by randomly generating $Ti_{11}Ni_{14}$ particles with a radius $r_o = 5\Delta r$ (Δr is the unit length of the grid) in a TiNi matrix (see Fig. 5(a)). The matrix had a concentration $C_m = 0.43$ and the value of the matrix's structural order parameters were zero. The concentration of the $Ti_{11}Ni_{14}$ particles was $C_p = 0.38$ and their structural order

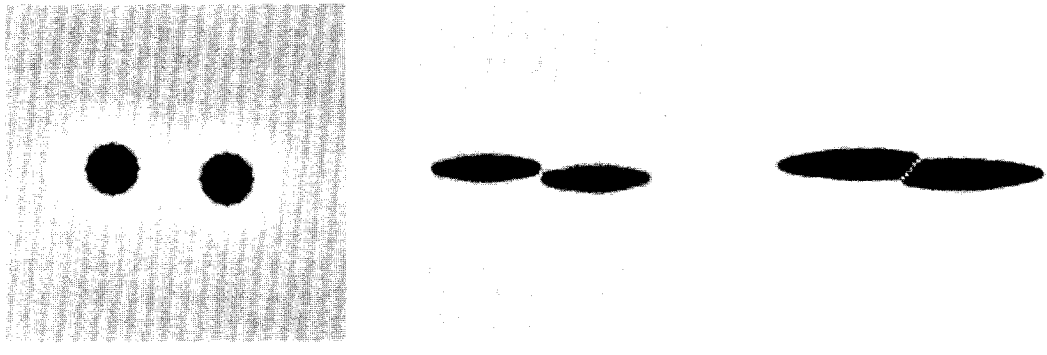

Fig. 3. The growth of a pair of conjugate $Ti_{11}Ni_{14}$ variant particles whose $[111]_{Ti_{11}Ni_{14}}$ axes are parallel to $[111]_{B2}$ and $[\bar{1}\bar{1}\bar{1}]_{B2}$ directions, respectively. The particles did not coalesce and are separated by an antiphase boundary. (a) $t^* = 0$, (b) $t^* = 1.9 \times 10^3$, (c) $t^* = 4.7 \times 10^3$.

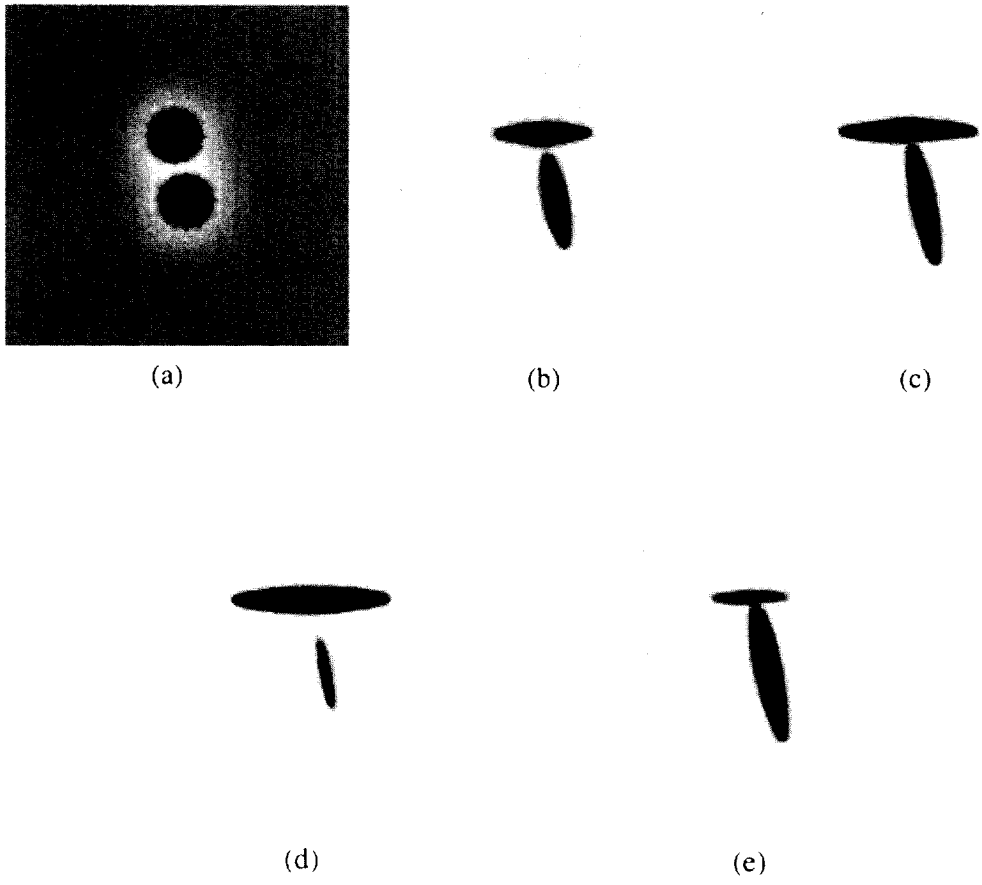

Fig. 4. The growth of two $Ti_{11}Ni_{14}$ variant particles whose $[111]_{Ti_{11}Ni_{14}}$ axes are parallel to $[111]_{B2}$ and $[1\bar{1}1]_{B2}$ directions, respectively. (a) $t^* = 0$, (b) $t^* = 1.9 \times 10^3$, (c) $t^* = 4.7 \times 10^3$. The growth of the particles became selective under applied strain constraints. (d) under a tensile strain applied along the x-axis, (e) under a compressive strain applied along the x-axis.

parameters had the equilibrium value of ± 1.0 whose sign distinguish a variant and its conjugate variant (e.g. the variant with its $[111]_{Ti_{11}Ni_{14}}$ parallel to $[111]_{B2}$ and the other with its $[111]_{Ti_{11}Ni_{14}}$ parallel to $[\bar{1}\bar{1}\bar{1}]_{B2}$). The system was initially in a non-equilibrium state and its microstructure varied with the "ageing" time to approach its equilibrium state. During the process, $Ti_{11}Ni_{14}$ particles grew and their shape changed from sphere (circle in 2D) to the lens-like disc with bamboo leaf-like cross-section. This simulated microstructural pattern is consistent with TEM observation as shown by Fig. 5(e). Comparing with the TEM micrograph, one may see that the present simulation characterizes the major feature of a multi-variant $Ti_{11}Ni_{14}$–TiNi system free from external constraints.

In a multi-variant system, the growth of different precipitate variants and their mutual positions are strongly affected by long-range elastic interactions between the variants. As a result, the precipitate variants should distribute in such a way that the elastic energy is reduced to minimum. The system under study has an initial microstructural pattern as Fig. 6(a) illustrates. Such a microstructure was unstable and it evolved to reduce the total free energy. The entire "ageing" process is illustrated in Fig. 6, which demonstrates that as the "ageing" time increased, some of the particles grew and the rest shrank or disappeared. The particles underwent significant shape changes and a rearrangement to minimize the total free energy of the system, resulting in a so called self-accommodative mutual arrangement of $Ti_{11}Ni_{14}$ precipitate variants. The bulk chemical energy, the elastic energy, the interphase boundary energy, and the total free energy of the system with respect to the "ageing" time are illustrated in Fig. 7. Curve 3 represents the total elastic energy of the system. As we can see in Fig. 7, the total elastic energy of the initial microstructure is very high, and it decreases as time increases. Curves 2 and 4 represent the total chemical free energy F_c and the interphase boundary energy σ_{tot}, respectively given by equations (2) and (3). Although they decrease over a long-period of time, one may notice small increases in the total chemical free energy and the interphase boundary energy during the intermediate stage of ageing. However,

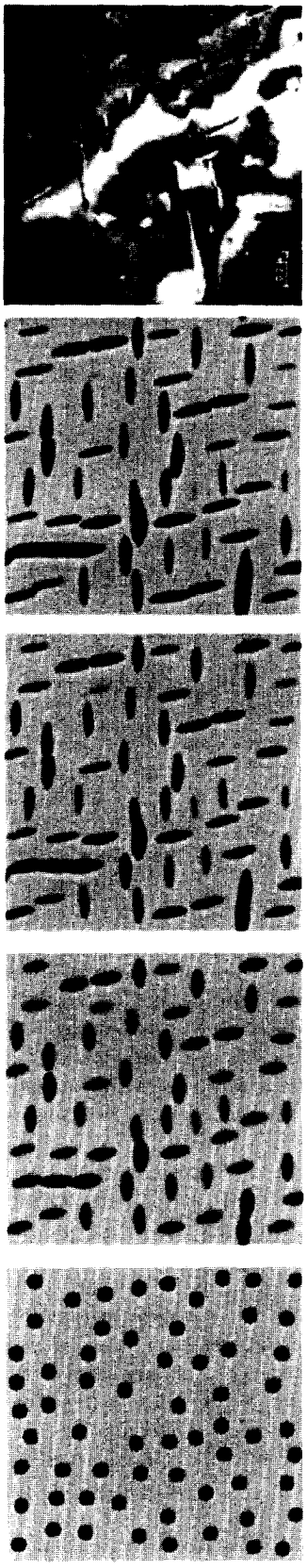

Fig. 5. Microstructural evolution in a multi-variant $Ti_{11}Ni_{14}$–TiNi system. (a) $t^* = 0$, (b) $t^* = 2.8 \times 10^3$, (c) $t^* = 6.6 \times 10^3$, (d) $t^* = 9.4 \times 10^3$, and (e) a TEM micrograph of Ti–51.5 at.% Ni alloy.

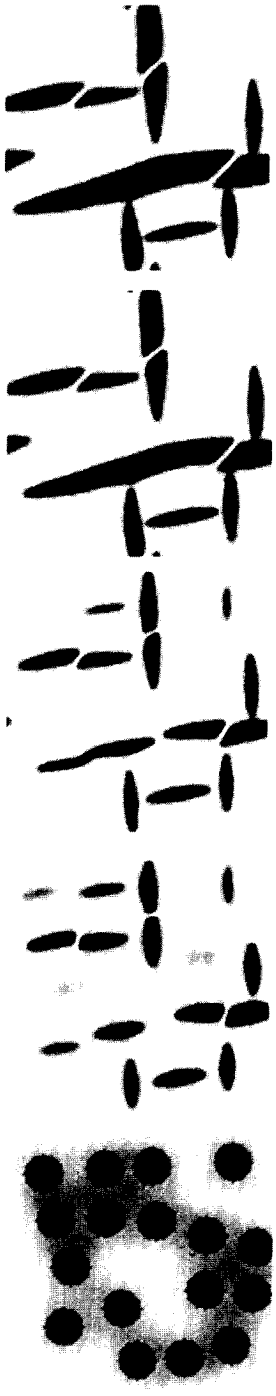

Fig. 6. The mutual arrangement of $Ti_{11}Ni_{14}$ variant particles is controlled by the coherent elastic strain energy. (a) $t^* = 1.9 \times 10^2$, (b) $t^* = 5.7 \times 10^3$, (c) $t^* = 9.4 \times 10^3$, (d) $t^* = 1.5 \times 10^4$ and (d) $t^* = 2.1 \times 10^4$.

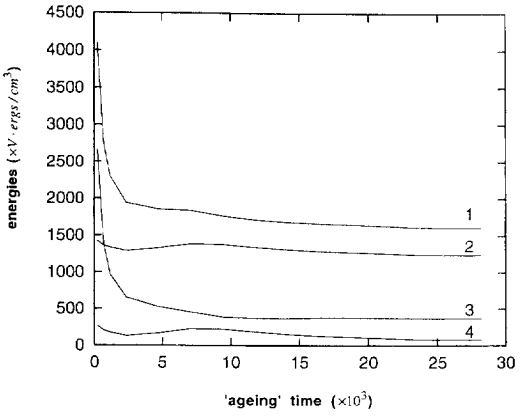

Fig. 7. Various energy components vs the "ageing" time. 1–the total free energy; 2–the chemical free energy F_c; 3–the total elastic energy; 4–the interphase boundary energy. The energies correspond to the morphological evolution illustrated in Fig. 6. V is the total volume of the system under study.

the total free energy of the system (curve 1) always decreases as a function of time.

The equilibrium concentrations of the $Ti_{11}Ni_{14}$ precipitate and the TiNi matrix in stress-free condition were determined as $C_1 = 0.443$ and $C_2 = 0.384$; while these concentrations changed to $C_1 = 0.431$ and $C_2 = 0.376$ when the elastic energy contribution is included. The elastic energy produces changes in the equilibrium compositions.

As demonstrated in the case of a single variant [7] or a two-particle system illustrated earlier, the growth of a variant is affected by applied strain or stress. This effect is attributed to the coupling between the applied strain/stress and the local strain. The elastic coupling changes the strain energy-barrier to the growth of coherent precipitate variants, and thus results in the selective variant growth. Previous calculation by Li and Chen [2] has demonstrated that even when the applying direction of a compressive strain deviates from the normal of the variant, the growth of the variant is still favored if the angle between the compressive strain and the normal to the variant is less than about fifty degrees. A tensile strain has an opposite effect on the variant growth. The calculation results were confirmed by the simulation of a single variant growth [7]. In the case of multi-variant system, an applied strain may promote the growth of some variants and retard the others, depending on their orientations. This strain-orienting effect results in selective $Ti_{11}Ni_{14}$ variant growth. Figure 8(a) illustrates a microstructure resulted from the selective variant growth under a compressive strain which was applied in the x direction (i.e. horizontally). The initial microstructure is similar to that shown by Fig. 5(a). Under the compressive strain, not all variants grew, and the grown variants were only those which had their normals parallel to the compressive strain. When a tensile strain was applied, however, the growth of these variants was unfavored, but other variants having their normals nearly perpendicular to the tensile strain were favored to grow. The resultant microstructure under the tensile strain is illustrated in Fig. 9(a). The strain-oriented precipitation of $Ti_{11}Ni_{14}$ variants demonstrated by the present simulation agrees very well with both experimental observation (see Fig. 8(b) and Fig. 9(b)) and the theoretical calculation presented in a previous paper [2]. Similar phenomena of the selective precipitation was also observed in other systems, e.g. the precipitation of disk-like α'' ($Fe_{16}N_2$) from a supersaturated Fe–N alloy. The α'' disk causes a compressive strain parallel to its normal, which is significantly larger than other strain components. When a tensile stress (similar to the effect of applied strain) is applied parallel to the normal to this variant, nucleation and growth of the variant is greatly promoted, against others which oriented in different crystallographic directions [31, 32].

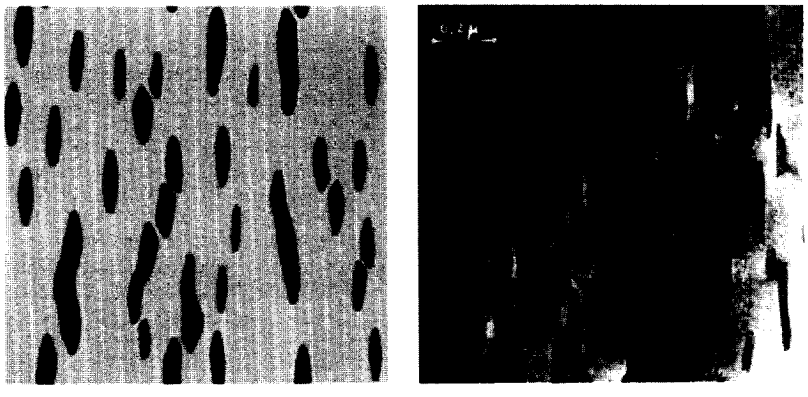

(a) (b)

Fig. 8. (a) the selective variant growth under a compressive strain, applied in the x-direction (i.e. the horizontal direction). Only those variants whose normals were parallel to the strain were favored to grow; (b) TEM observation of the strain-oriented $Ti_{11}Ni_{14}$ precipitation in Ti–51.5 at.% Ni alloy under a compressive strain constraint applied along the x-axis.

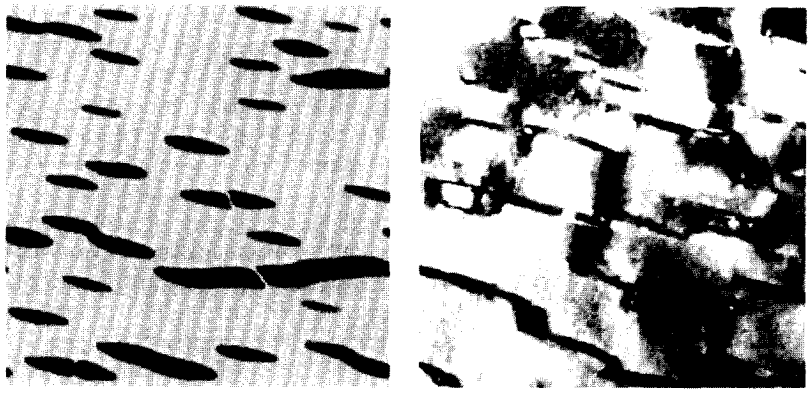

(a) (b)

Fig. 9. (a) the selective variant growth under a tensile strain, applied in the x-direction. Only one type of variant grew whose normals are near perpendicular to the tensile stress; (b) TEM observation of the strain-oriented $Ti_{11}Ni_{14}$ precipitation in Ti–51.5 at.% Ni alloy under a tensile strain constraint applied closely along the x-axis.

6. CONCLUSION

A computer simulation study was conducted to investigate coherent $Ti_{11}Ni_{14}$ precipitation in TiNi shape memory alloys and the selective variant growth of $Ti_{11}Ni_{14}$ precipitates under applied strain-constraints. A time-dependent Ginzburg–Landau kinetic model was employed, taking into account the effect of applied strain on the elastic strain energy of the system. It was demonstrated that the growth of lens-like $Ti_{11}Ni_{14}$ precipitates in a supersaturated TiNi matrix is strongly affected by internal and external strains. The morphology of the precipitate and the mutual arrangement of different $Ti_{11}Ni_{14}$ variants are determined by the coherent elastic energy. Under the influence of external strain constraint, the distribution of $Ti_{11}Ni_{14}$ variants becomes anisotropic, resulting in parallel alignment of $Ti_{11}Ni_{14}$ precipitate variants. Excellent agreement between the simulation and experimental observations was found.

Acknowledgements—This work is supported by the Office of Naval Research Young Investigator Program under the grant number N-00014-95-1-0577. The simulation was performed at the Pittsburgh Super-computing Center.

REFERENCES

1. I. Kainuma, R., Matsumoto, M. and Honma, T., in *ICOMAT-86*. The Japan Inst. of Metals, Aoba Aramaki, Sendai 980, Japan, 1987, 717.
2. Li, D. Y. and Chen, L. Q., *Acta mater.*, 1997, **45**, 471.
3. Khachaturyan, A. G., *Theory of Structural Transformations in Solids*. John Wiley & Sons. Inc., New York, 1983.
4. Porter, D. A. and Easterling, K. E., *Phase Transformations in Metals and Alloys*. Van Nostrand Reinhold Co., 1989.
5. Honma, T., in *ICOMAT-86*, The Japan Inst. of Metals, Aoba Aramaki, Sendai 980, Japan, 1987, 703.
6. Kaneko, K., Uehara, M., Aoki, H., Kubo, M., Suzuki, T. and Yoshida, A., *J. Soc. Mater. Sci., JPN*, 1993, **42**, 1103.
7. Li, D. Y. and Chen, L. Q., *Acta mater.* **45**, 2435.
8. Wang, Y., Wang, H-Y., Chen, L. Q. and Khachaturyan, A. G., *J. Am. Ceram. Soc.*, 1995, **78**, 657.
9. Fan, Danan and Chen, L. Q., *J. Am. Ceram. Soc.*, 1995, **78**, 769.
10. Chandra, K. and Purdy, G. R., *J. Appl. Phys.*, 1968, **39**, 2176.
11. Nishida, M., Wayman, C. M., Kainuma, R. and Honma, T., *Script. metall.*, 1986, **20**, 899.
12. Saburi, T., Nenno, S. and Fukuda, T., *Proc. XIth Int. Conf. On Electron Microscopy*, Kyoto, 1986, 1631.
13. Eshelby, J. D., *Proc. Roy. Soc.*, 1957, **A241**, 376.
14. Eshelby, J. D., *Proc. Roy. Soc.*, 1959, **A252**, 561.
15. Khachaturyan, A. G., *Sov. Phys. - Solid State*, 1967, **8**, 2163.
16. Khachaturyan, A. G. and Shatalov, G. A., *Sov. Phys. JETP*, 1969, **29**, 557.
17. Walpole, L. J., *Proc. Roy. Soc.*, 1967, **A300**, 270.
18. Kinoshita, N. and Mura, T., *Phys. Stat. Solidi (a)*, 1971, **5**, 759.
19. Asaro, R. J. and Barnett, D. M., *J. Mech. Phys. Solids*, 1975, **23**, 77.
20. Mura, T., Mori, T. and Kato, M., *J. Mech. Phys. Solids*, 1976, **24**, 305.
21. Lee, J. K., Barnett, D. M. and Aaronson, H. I., *Metall. Trans.*, 1977, **8A**, 963.
22. Mori, T., Cheng, P. C., Kato, M. and Mura, T., *Acta Metall.*, 1978, **26**, 1435.
23. Khachaturyan, A. G., Semenovskaya, S. and Tsakalakos, T., *Phys. Rev.*, 1995, **B52**, 1.
24. Chen, L-Q., Wang, Y. and Khachaturyan, A. G., *Phil. Mag. lett.*, 1992, **65**, 15.
25. Wang, Y., Chen, L. Q. and Khachaturyan, A. G., Modeling of dynamical evolution of micro/mesoscopic morphological patterns in coherent phase transformations, in *Computer Simulation in Materials Science, Nano/Meso/Macroscopic Space and Time Scales*. NATO Advanced Study Institute Series. edited by H. O. Kirchner, *et al.* Kluwer Academic Publishers, Dordrecht. p. 325, 1996.
26. Cahn, J. W. and Hilliard, J. E., *J. Chem. Phys.*, 1958, **28**, 258.
27. Allen, S. M. and Cahn, J. W., *Acta Metall.*, 1979, **27**, 1085.

28. Mercier, O., Melton, K. N., Gremaud, G. and Hägi, J., *J. Appl. Phys.*, 1980, **51**(3), 1833.
29. Academician Fedor I. Fedorov. *Theory of Elastic Waves in Crystals*. Plenum Press, New York, 1968.
30. Chen, L. Q. and Shen, J., to be published.
31. Nakada, Y., Leslie, W. C. and Chray, T. P., *Trans. Amer. Soc. Metals*, 1967, **60**, 223.
32. Tanaka, Y., Sato, A. and Mori, T., *Acta Metall.*, 1978, **26**, 529.

APPENDIX A—ELASTIC ENERGY CALCULATION

The local elastic strain in a two-phase mixture is the difference between the total strain and the stress-free strain, that is

$$\varepsilon_{ij}^{el}(\mathbf{r}) = \varepsilon_{ij}(\mathbf{r}) - \varepsilon_{ij}^{0}(\mathbf{r}) = \varepsilon_{ij}(\mathbf{r}) - \sum_p \varepsilon_{ij}^{0}(\mathbf{r})\eta_p^2(\mathbf{r}). \tag{A1}$$

In the homogeneous modulus approximation (i.e. the elastic modulus of the precipitate phase is the same as that of the matrix), the elastic stress field is given by

$$\sigma_{ij} = C_{ijkl}\varepsilon_{kl}^{el}(\mathbf{r}) = C_{ijkl}\left[\varepsilon_{kl}(\mathbf{r}) - \sum_p \varepsilon_{kl}^{0}(\mathbf{r})\eta_p^2(\mathbf{r})\right] \tag{A2}$$

where C_{ijkl} is the elastic constant. The equilibrium condition gives

$$\frac{\partial \sigma_{ij}(\mathbf{r})}{\partial r_j} = C_{ijkl}\left[\frac{\partial \varepsilon_{kl}(\mathbf{r})}{\partial r_j} - \sum_p \varepsilon_{kl}^{0}(p)\frac{\partial}{\partial r_j}\left(\eta_p^2(\mathbf{r})\right)\right] = 0. \tag{A3}$$

Following Khachaturyan, the total strain $\varepsilon_{ij}(\mathbf{r})$ may be represented as the sum of homogeneous and heterogeneous strains:

$$\varepsilon_{ij}(\mathbf{r}) = \bar{\varepsilon}_{ij} + \delta\varepsilon_{ij}(\mathbf{r}) \tag{A4}$$

where the homogeneous strain, $\bar{\varepsilon}_{ij}$, is defined so that

$$\int_V \delta\varepsilon_{ij}(\mathbf{r})d^3\mathbf{r} = 0. \tag{A5}$$

The homogeneous strain is the uniform macroscopic strain, while the heterogeneous strain is chosen such that it has no macroscopic effects. The heterogeneous strain can be expressed in terms of heterogeneous displacement,

$$\delta\varepsilon_{kl}(\mathbf{r}) = \frac{1}{2}\left[\frac{\partial u_k(\mathbf{r})}{\partial r_l} + \frac{\partial u_l(\mathbf{r})}{\partial r_k}\right]. \tag{A6}$$

Substitute (A4) and (A6) into (A3), we have

$$C_{ijkl}\frac{\partial^2 u_k(\mathbf{r})}{\partial r_j \partial r_l} = \sum_p \sigma_{ij}^{0}(p)\frac{\partial}{\partial r_j}\left(\eta_p^2(\mathbf{r})\right) \tag{A7}$$

where, $\sigma_{ij}^{0}(p) = C_{ijkl}\varepsilon_{kl}^{0}(p)$. Equation (A7) can be readily solved in the Fourier space,

$$v_k(\mathbf{g}) = -iG_{ik}(\mathbf{g})\sum_p \sigma_{ij}^{0}(p)g_l\left\{\eta_p^2(\mathbf{r})\right\}_{\mathbf{g}} \tag{A8}$$

where $\mathbf{g}$ is a reciprocal lattice vector, g_j is the jth component of $\mathbf{g}$,

$$v_k(\mathbf{g}) = \int_V u_k(\mathbf{r})e^{-i\mathbf{g}.\mathbf{r}}d^3\mathbf{r} \tag{A9}$$

$$\left\{\eta_p^2(\mathbf{r})\right\}_{\mathbf{g}} = \int_V \eta_p^2(\mathbf{r})e^{-i\mathbf{g}.\mathbf{r}}d^3\mathbf{r} \tag{A10}$$

and $G_{ik}(\mathbf{g})$ is the inverse tensor to $(G^{-1}(\mathbf{g}))_{ik} = C_{ijkl}g_jg_l = g^2 C_{ijkl}n_jn_l = g^2\,\Omega_{ik}^{-1}(\mathbf{n})$, where $\mathbf{n} = \mathbf{g}/g$.

The total elastic energy of a coherent multi-variant mixture is given by

$$E_{el} = \frac{1}{2}\int_V C_{ijkl}\varepsilon_{ij}^{el}(\mathbf{r})\varepsilon_{kl}^{el}(\mathbf{r})d^3\mathbf{r}. \tag{A11}$$

Using the definitions (A1), (A4), (A6), and (A7), the elastic energy can be written as

$$\begin{aligned} E_{el} = {} & \frac{V}{2}C_{ijkl}\bar{\varepsilon}_{ij}\bar{\varepsilon}_{kl} - V\sum_p \bar{\varepsilon}_{ij}\sigma_{kl}^{0}(p)\overline{\eta_p^2(\mathbf{r})} \\ & + \frac{V}{2}C_{ijkl}\sum_p\sum_q \varepsilon_{ij}^{0}(p)\varepsilon_{kl}^{0}(q)\overline{\eta_p^2(\mathbf{r})\eta_q^2(\mathbf{r})} \\ & + \int_V\left[\frac{1}{2}C_{ijkl}\frac{\partial u_i}{\partial r_j}\frac{\partial u_k}{\partial r_l} - \sum_p \sigma_{ij}^{0}(p)\frac{\partial u_i}{\partial r_j}\eta_p^2(\mathbf{r})\right]d^3\mathbf{r} \end{aligned} \tag{A12}$$

where $(\overline{\cdots})$ represents the volume average of $(\ldots)$ and V is the total volume of the system. Substitution of the back Fourier transforms of $\mathbf{u}(\mathbf{r})$ and $\eta_p^2(\mathbf{r})$ into (A12), we obtain the final form of the total elastic strain energy of the multi-variant mixture

$$\begin{aligned} E_{el} = {} & \frac{V}{2}C_{ijkl}\bar{\varepsilon}_{ij}\bar{\varepsilon}_{kl} - VC_{ijkl}\bar{\varepsilon}_{ij}\sum_p \varepsilon_{kl}^{0}(p)\overline{\eta_p^2(\mathbf{r})} \\ & + \frac{V}{2}C_{ijkl}\sum_p\sum_q \varepsilon_{ij}^{0}(p)\varepsilon_{kl}^{0}(q)\overline{\eta_p^2(\mathbf{r})\eta_q^2(\mathbf{r})} \\ & - \frac{1}{2}\sum_p\sum_q\int\frac{d^3\mathbf{g}}{(2\pi)^3}B_{pq}(\mathbf{n})\left\{\eta_p^2(\mathbf{r})\right\}_{\mathbf{g}}^{*}\left\{\eta_q^2(\mathbf{r})\right\}_{\mathbf{g}} \end{aligned} \tag{A13}$$

where

$$B_{pq}(\mathbf{n}) = n_i\sigma_{ij}^{0}(p)\Omega_{jk}(\mathbf{n})\sigma_{kl}^{0}(q)n_l. \tag{A14}$$